Ion-beam modification of Co/Ag multilayers I: Structural evolution and magnetic response

T. Veres, M. Cai, R. W. Cochrane, and S. Roorda

Citation: J. Appl. Phys. **87**, 8504 (2000); doi: 10.1063/1.373570
View online: http://dx.doi.org/10.1063/1.373570
View Table of Contents: http://jap.aip.org/resource/1/JAPIAU/v87/i12
Published by the American Institute of Physics.

Ion-beam modification of Co/Ag multilayers I: Structural evolution and magnetic response

T. Veres, M. Cai, R. W. Cochrane,[a] and S. Roorda
Département de physique et Groupe de recherche en physique et technologie des couches minces, Université de Montréal, C.P. 6128, Succ. Centre-ville, Montréal, Québec H3C 3J7, Canada

(Received 18 June 1999; accepted for publication 20 March 2000)

We describe the effects of 1 MeV Si^+ ion-beam irradiation on a sputtered Co/Ag multilayer with layer thicknesses of 5 Å for Co and 25 Å for Ag, thicknesses for which the magnetoresistance is maximum in the as-deposited sample. X-ray diffraction, magnetization, and magnetoresistance measurements all point to the conclusion that the Co is initially dispersed through the Ag and segregates completely upon ion-beam bombardment. Throughout the process both Ag and Co grains maintain a high degree of texture, essentially face centered cubic (111). The magnetization behavior evolves from superparamagnetic to mixed superparamagnetic–ferromagnetic with ion dose whereas the room-temperature magnetoresistance decreases from 12% to 1.5% upon irradiation up to 5×10^{16} Si^+/cm^2. Simple models taking into account the size distribution of the Co particles have been used to analyze these phenomena in order to quantify the particle size distribution. © *2000 American Institute of Physics.* [S0021-8979(00)09512-8]

I. INTRODUCTION

Over the past few years, discontinuous multilayers and heterogeneous mixtures of magnetic and nonmagnetic metals have been extensively studied because of their unique magnetic and transport properties, in particular, the phenomenon of giant magnetoresistance (GMR) which has great potential for application in magnetic recording technology.[1–5] In these systems, the magnetic material is heterogeneously dispersed in the nonmagnetic matrix, forming single-domain particles ranging in size from a few to many thousands of atoms. The magnetic properties of these materials are complex; ferromagnetic, superparamagnetic, or spin-glass behavior can be obtained depending on the sizes and separations of the magnetic particles. Specifically, the size distribution of the magnetic particles is one of the key parameters for the appearance of the GMR in these materials.[6–8]

The Co/Ag system is an excellent example of such materials and has been widely studied. In equilibrium, Co and Ag are completely immiscible due, in part, to the fact that the surface free energy[9] of Co (2.71 J/m^2) is more than twice that of Ag (1.30 J/m^2) and, in part, to the large atomic size difference. Face-centered-cubic (fcc) Ag has a lattice parameter that is 15% larger than that of fcc Co. As a result, the heat of formation between Co and Ag is strongly positive ($\Delta H_m = +26$ kJ/g atom) so there is no tendency for alloying. In most of the research to date, Co/Ag mixtures have been prepared by co-deposition at elevated temperatures or at room temperature and subsequently annealed in order to control the magnetic-particle size. These materials exhibit a maximum GMR for mixtures around 30 at. % Co.[10]

Depending on the ion, its energy and dose, ion bombardment can promote local atomic diffusion and is thus capable of modifying the microstructure of alloys. Such changes are strongly dependent on the details of the chemical interactions between the constituents, their miscibility and heats of formation.[11–13] Of particular interest is how such ion-beam modification affects the magnetic behavior of alloys and multilayers, particularly those exhibiting GMR for which only a few studies have been reported.[14,15] Recently, we studied the effect of low-temperature ion-beam mixing on the GMR in Co/Cu multilayers.[16] These results demonstrate that 1 MeV Si^+ irradiation at 77 K provides a sensitive tool for structural modification on a nanometric scale for films much thinner than the ion range.

Because the size distribution of the magnetic particles plays such a central role in the magnetic behavior of heterogeneous systems, it is important to follow the magnetic properties through various stages of magnetic-particle formation. With this objective, we have undertaken a systematic examination of the evolution of the microstructure and the magnetic behavior of Co/Ag multilayer mixtures resulting from 1 MeV Si^+ ion bombardment. Samples were deposited with nominal Co-layer thicknesses ranging from 2 to 15 Å with a constant Ag layer thickness of 25 Å and studied as a function of ion dose. This article presents results on a single sample with a nominal Co thickness (t_{Co}) of 5 Å for which the initial room-temperature GMR is a maximum ($\Delta\rho/\rho = 11.9\%$). Emphasis is placed here on the analysis of the effects of ion irradiation on the size distribution of the Co particles and their influence on the structural, magnetic, and magnetoresistance properties. Data for the entire series will be published elsewhere.[17]

II. EXPERIMENTAL DETAILS

Co/Ag multilayers were deposited onto SiO_2 layers thermally grown on Si (001) substrates using a modified single-source rf triode sputtering system with a base pressure of 1×10^{-7} Torr.[18] Samples were sputtered under a pressure of 4

[a]Electronic mail: cochrane@ere.umontreal.ca

mTorr of argon gas (99.999%) and a rf power of 100 W resulting in sputtering rates of 0.9 Å/s for Co and 5.1 Å/s for Ag. During sputtering, the substrate temperature was maintained at about 40 °C. Layer thicknesses were computer controlled during deposition and subsequently confirmed with a DEKTAK step profiler. Crystallographic structures were investigated by x-ray diffraction using a Cu $K\alpha$ source. Magnetic moments were measured at room temperature using a vibrating sample magnetometer operating at 85 Hz with the external field applied in the sample plane. Magnetic measurements below room temperature were taken with the aid of a custom-modified Quantum Design Model 6000 Physical Property Measurement System. Resistance and magnetoresistance were obtained by a standard four-point method on a high-resolution ac bridge[19] with fields applied both in the sample plane and perpendicular to it.

Normal incidence ion-beam irradiation was performed in a vacuum of about 1×10^{-7} Torr with 1 MeV Si^+ ions rastered over the entire sample surface. To avoid sample heating during irradiation, the ion beam current was kept below 50 nA/cm^2 and the samples were placed in thermal contact with a copper block maintained at 77 K. At each stage, the irradiation was performed on a single SiO_2[Ag50 Å(Co5 Å/Ag25 Å)$_{70}$] multilayer; the dose was systematically increased from an initial value of 1×10^{13} Si^+ cm^{-2} ($\sim$0.009 displacements per atom, dpa) to 5×10^{16} Si^+ cm^{-2} ($\sim$32 dpa). The ion energy (1 MeV) was selected such that its projected range was greater than the total film thickness (2000 Å) in order to give a uniform damage profile throughout the multilayer. Only a very small amount ($<$0.1%) of the implanted ions were expected to remain within the magnetic films, the rest being transmitted or backscattered.

III. RESULTS

A. X-ray diffraction

X-ray diffraction spectra of the sample after different ion doses are plotted in Fig. 1 along with the spectrum for the bare substrate which serves to demonstrate that the structure around $2\theta=33°$ arises from the substrate. Since the region $55°<2\theta<75°$ is dominated by substrate peaks, it has been omitted from the figure. Nevertheless, the substrate lines did prove to be useful for correcting small variations in the sample alignment ($\Delta(2\theta)<0.2°$).

1. Microstructure of the as-deposited sample

For the as-deposited sample, only two broad principal peaks are observed and indexed as the (111) and (222) reflections of fcc Ag, indicating that the Ag is highly textured with its close-packed plane parallel to the substrate. Despite the strong tendency for phase separation between Co and Ag, no evidence of either pure fcc or hexagonal-close-packed (hcp) Co is found in this sample. The first order Ag peak contains considerable structure: a central peak at 39.0°, a sharp shoulder at 38.2°, and small subpeaks around 36° and 42.5°. The sharp shoulder is situated almost exactly at the (111) position for pure bulk Ag, whereas the principal peak corresponds to a compression of some 2.4% with respect to the bulk reflection. Given the 15% lattice mismatch with fcc

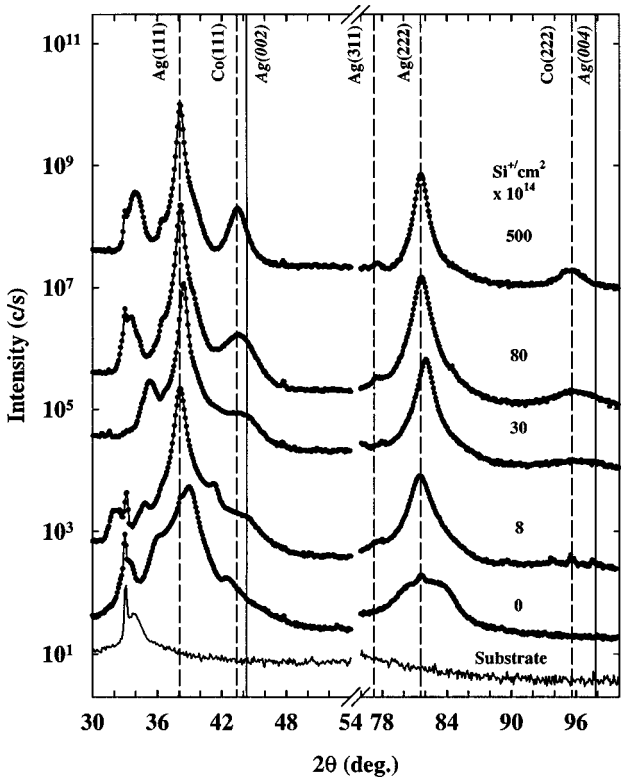

FIG. 1. Selected high-angle x-ray diffraction patterns measured with Cu $K\alpha$ radiation on a [50 Å (Co5 Å/Ag25 Å)$_{70}$] multilayer irradiated with 1 MeV Si^+ ions. The solid-line spectrum originates from the substrate. For clarity, successive diffraction patterns have been shifted vertically.

Co, the position of this peak corresponds to that expected for a mixture of Co_5Ag_{25}, the composition of our sample. The two satellite lines can be analyzed as superlattice reflections around the principal peak at 39.0° arising from a periodic structure with a wavelength of 29 Å. Finally, the second order peak around 82° shows a weak narrow line at the (222) position of bulk Ag on top of a broad peak shifted to higher angles; no superlattice substructure is observed around this reflection.

These data lead to a relatively simple picture of the microstructure of the as-deposited sample. In the buffer layer and possibly the first few periods, Ag takes up a near equilibrium configuration. At 5 Å thickness, the Co grows on Ag in a discontinuous layer of small three-dimensional islands. The heavier Ag atoms disperse the small Co clusters throughout the Ag layer, resulting in a smaller average lattice parameter for the mixture. The Co dispersion is clearly nonuniform as indicated by the relatively broad first and second order peaks and the persistence of the 29 Å period. Nonetheless, the Co is finely enough dispersed so that the average lattice parameter of the mixture is shifted and no pure Co peak is observed. The entire sample maintains a high degree of fcc (111) texture.

2. Evolution of the microstructure with ion dose

A significant structural evolution results from the ion-beam irradiation.

(a) Both the first and second order (111) Ag peaks shift to lower angles and narrow considerably. The monotonic line

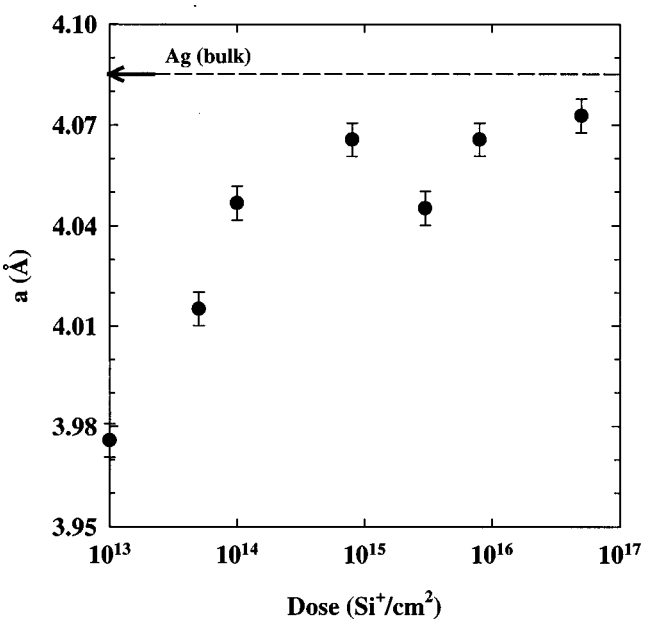

FIG. 2. The variation of the lattice parameter of the Ag grains of the [50 Å(Co5 Å/Ag25 Å)$_{70}$] multilayer as a function of the irradiation dose.

narrowing and accompanying intensity increase of these peaks with ion dose indicates systematic growth of the Ag grains. Also, as presented in Fig. 2, the Ag lattice parameter, as calculated from the peak position, rises very close to the room temperature bulk value for pure Ag of 4.086 Å.

(b) Two new lines appear, centered at $2\theta = 43.4°$ and 95.5°. A detailed analysis of these peaks leads to the conclusion that they cannot be assigned as fcc Ag (200) and (400) on the basis of a lattice parameter consistent with Fig. 2. They must arise from a Co-dominated phase and be designated either (111) and (222) fcc lines with a cube edge of 3.60 Å or hcp (002) and (004) with a *c*-axis parameter of 4.16 Å. These values are some 2% larger than those for bulk Co but are identical to the ones reported by Mitchell and co-workers[20] for co-deposited CoAg alloys with average compositions similar to that of our sample.

(c) The superlattice structure is slightly enhanced up to a dose of 8×10^{14} Si^+/cm^2; subsequent irradiation suppresses it completely.

(d) The high degree of texture for both the Ag and the Co remains almost complete up to the highest dose of 5×10^{16} Si^+/cm^2.

The assignment of the lines at $2\theta = 43.4°$ and 95.5° to Co clusters is also supported by the fact that the intensities of these subsidiary peaks increase in other samples with thicker Co layers.[17] Taken together with the evolution of the Ag peaks, it is clear that energetic ion irradiation has induced almost complete demixing of the Co atoms from the Ag matrix. Using Scherrer's formula,[21] the average Co grain size in the growth direction has been estimated from the linewidths of these peak; the values are listed in Table I. One calculates a grain size of 36 Å after irradiation with 8×10^{14} Si^+/cm^2 which increases to 67 Å after a dose of 5×10^{16} Si^+/cm^2. These dimensions are consistent with those found from the analysis of the magnetic data as described in the following sections.

TABLE I. The average diameter of Co particles obtained from fits to the magnetization at room temperature, $M(H)$, the zero-field cooled magnetization measurements, ZFC, the magnetoresistance, MR(H), and from the application of the Scherrer formula to the x-ray diffraction peaks.

Dose (10^{14} Si^+/cm^2)	D_m (Å) $M(H)$	D_m (Å) ZFC	D_m (Å) MR(H)	ξ(Å) (Scherrer)
0	39±0.6	54±2	23±0.5	···
8.0	34±0.3	52±2	26±0.3	···
30	36±0.6	···	30±0.8	36±5
80	44±0.3	66±4	37±0.4	53±4
100	47±0.8	···	45±0.4	···
500	54±0.7	···	52±0.9	67±4

B. DC magnetization measurements

Figure 3 shows low field in-plane magnetic moment-field curves measured at 300 K at various stages of ion irradiation. Initially, the magnetic moment displays a slow single-valued rise toward saturation as a function of the applied magnetic field. A dose of 8×10^{14} Si^+/cm^2 induces a reduction in the initial field slope of the moment although the analysis described below indicates that the saturation value has increased. Upon further irradiation, the initial slope rises and the curve develops an hysteresis with a coercive field that increases with ion dose. The mixed hysteretic–anhysteretic behavior persists up to the maximum dose of 5×10^{16} Si^+/cm^2.

At this time there exists no unified model which can describe the combined hysteretic and anhysteretic magnetization curves obtained for systems of weakly interacting small magnetic particles. Consequently, we adopt the empirical approach of Stearns and Cheng[22] and analyze each magnetization curve as the sum of two contributions: a ferromagnetic one, $M_{\text{ferro}}(H)$, due to larger ferromagnetic grains or interacting particles (which are easily saturated) and a superparamagnetic one, $M_{\text{SP}}(H)$, arising from small noninteracting unblocked particles (which at room temperature require very large fields for saturation)

$$M(H) = M_{\text{ferro}}(H) + M_{\text{SP}}(H). \tag{1}$$

The ferromagnetic contribution can be represented by an analytical function describing the hysteretic behavior as a function of the coercive field H_c and the remanence M_r (Ref. 22)

$$M_{\text{ferro}}(H) = \frac{2M^0_{\text{ferro}}}{\pi}\tan^{-1}\left[\frac{H \pm H_c}{H_c}\tan\left(\frac{\pi M_r}{2M^0_{\text{ferro}}}\right)\right]. \tag{2}$$

Here M^0_{ferro} is the saturation value for the magnetic moment of the ferromagnetic part. Unfortunately, there is no unique relation between the size of the magnetic particles and the magnetic parameters H_c and M_r so that this description for the ferromagnetic fraction of the sample cannot be used to estimate the size distribution of the ferromagnetic particles.

For small Co particles, there is a critical size below which they form single magnetic domains. Below the block-

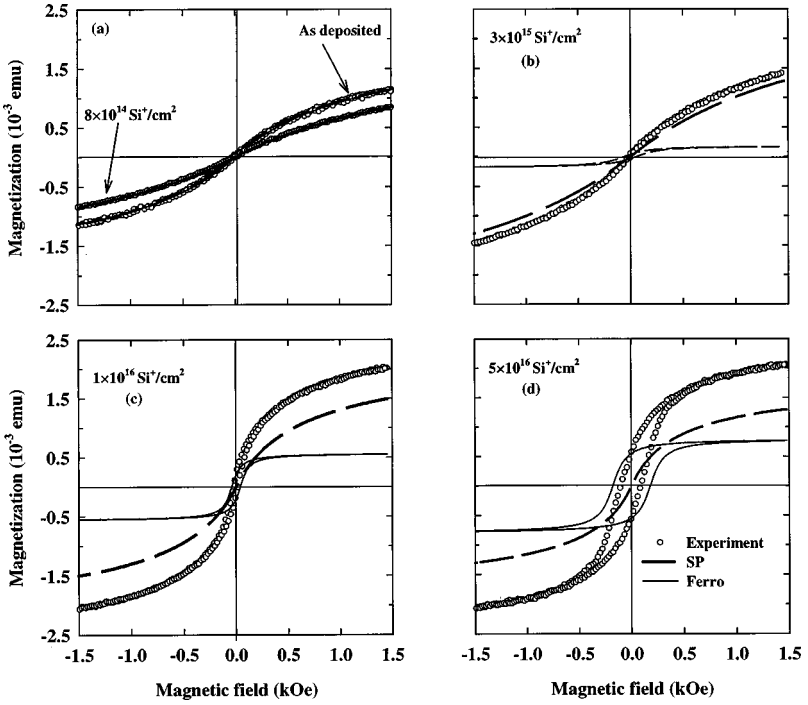

FIG. 3. Magnetization curves of the sample measured at room temperature after different irradiation doses. The measured data are represented by the open circles, the calculated superparamagnetic contribution by the dashed line and the calculated ferromagnetic contribution by the closed line.

ing temperature, T_b, the magnetic moment of a single-domain particle is frozen along a local easy axis determined by shape and strain anisotropies. Above T_b, the thermal energy is larger than the anisotropy energy and the moment becomes free to fluctuate. In this superparamagnetic state, the total moment of an ensemble of weakly interacting particles of uniform size can be described by the Langevin function.[23] However, for a realistic representation of the behavior of our samples we consider a distribution of particle sizes. In order to quantify this analysis, we follow the proposal of Chantrell *et al.*[24] and use a log–normal distribution for the volume of the magnetic particles. Assuming for simplicity that the particles are spherical ($V=\pi D^3/6$), the size distribution can be expressed in terms of the diameter D as

$$f(D)d(\ln D)=\frac{1}{\sqrt{2\pi}\sigma}\exp\left[-\frac{(\ln(D/D_m))^2}{2\sigma^2}\right]d(\ln D), \tag{3}$$

where D_m and σ are respectively the mean value and the variance of the size distribution. The superparamagnetic contribution to the total magnetic moment can then be expressed as

$$M_{\mathrm{SP}}(H)=M^0_{\mathrm{SP}}\int_{-\infty}^{\infty}L\left(\frac{\mu(D)H}{k_BT}\right)f(D)d(\ln D), \tag{4}$$

where $L(x)=\coth(x)-1/x$ is the Langevin function, $\mu=M_sV=\pi M_sD^3/6$ the magnetic moment of a particle with volume V and saturation magnetization $M_s=1420$ gauss and M^0_{SP} is the saturation value for the superparamagnetic contribution to the total magnetic moment. In order to evaluate the relative size of the ferromagnetic and superparamagnetic contributions, the magnetization curves were fitted to the model described by Eqs. (1)–(3). The superparamagnetic and ferromagnetic components of the magnetization curves so calculated are superimposed on the experimental data in Fig. 3.

The magnetic moment of the as-deposited sample shown in Fig. 3(a) rises gradually as a function of the applied field with no sign of saturation and very little hysteresis ($H_c<10$ Oe), a behavior that is characteristic of small superparamagnetic Co particles. As expected, the curve can be fitted without a ferromagnetic contribution, indicating that almost all the Co atoms are contained within small superparamagnetic particles. The deduced size distribution is described by a mean particle diameter of $D_m=39$ Å. This and subsequent values for the particle sizes are listed in Table I.

Under low dose irradiation, the magnetization curves preserve an essentially superparamagnetic behavior. The decrease in the low-field slope of the $M-H$ curve upon irradiation with 8×10^{14} Si^+/cm^2 is apparently due to a small decrease in the mean particle size at low doses. At a dose of 3×10^{15} Si^+/cm^2 [Fig. 3(b)], the presence of a small hysteresis reveals a ferromagnetic component along with the dominant superparamagnetic one: $M^0_{\mathrm{ferro}}/M^0_{\mathrm{SP}}=0.07$. At doses higher than 8×10^{15} Si^+/cm^2 [Figs. 3(c)–3(d)], the magnetization curves show pronounced hysteresis arising from a ferromagnetic component comparable in size to the superparamagnetic one. At 5×10^{16} Si^+/cm^2, $M^0_{\mathrm{ferro}}/M^0_{\mathrm{SP}}=0.45$; the average particle diameter deduced from the superparamagnetic component has grown to 54 Å but evidently remains smaller than the critical size for single-domain behavior. Nevertheless, the hysteresis in the magnetization curves is signaling the presence of large blocked particles or, at least, a significant ferromagnetic coupling between the Co particles.

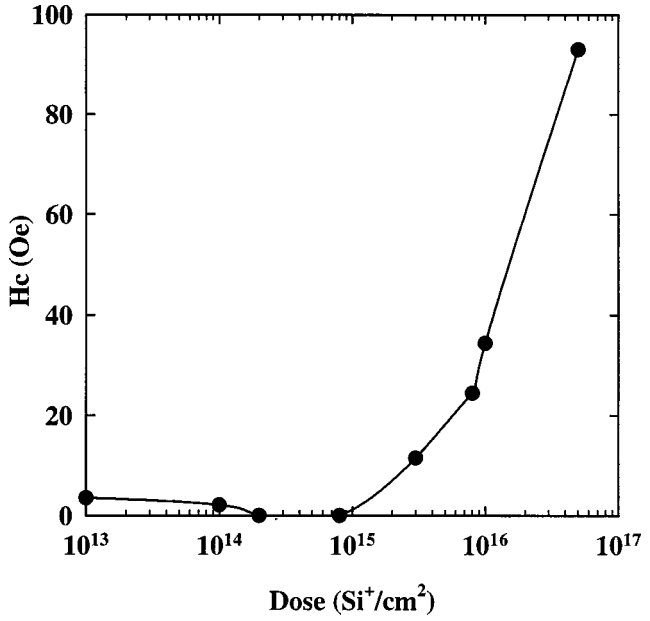

FIG. 4. Variation with ion dose of the coercive field for the [50 Å(Co5 Å/Ag25 Å)$_{70}$] multilayer.

C. Coercive field

The in-plane coercive field, measured at room temperature as a function of the ion dose, is presented in Fig. 4. Its rapid rise for doses above 10^{15} Si^+/cm^2 results from significant changes in the size, shape, and interparticle distances, and demonstrates a striking dependence of the coercive field on the sample morphology. It is known[25] that for large multidomain particles, small coercivities are associated with the relatively low energies necessary to activate domain-wall motion. Below a critical size, which depends on the material and the shape, the particles become single domain and only spin rotation processes can change the magnetization. Such spin rotation processes require larger energies than does domain-wall motion resulting in an increase in the coercive field. As the size of the single-domain particle is reduced from the critical value, the coercive field should decrease since the smaller moments are easier to activate thermally. On this basis, Fig. 4 indicates that, even at the largest dose, the mean particle size has not attained the critical value. A similar behavior of the coercive field has been observed upon annealing in Co_xCu_{1-x}, Fe_xCu_{1-x} alloys[26,27] and Co–Ag alloys deposited above room temperature.[28]

Another method for estimating single-domain particle sizes quantitatively is to determine the blocking temperature T_b for thermal activation of magnetization rotation. To this end, zero-field cooled (ZFC) and field-cooled (FC) magnetization measurements were performed after each irradiation. The sample was initially cooled to 5 K in ZFC or in the presence of the FC whereupon the magnetization at fixed applied field was measured as a function of increasing temperature. Both series of measurements were performed at fields of 10, 20, 40, and 70 Oe. The field-dependent blocking temperature is indicated by a peak in the ZFC curve and by the onset of irreversibility between the FC and ZFC curves.

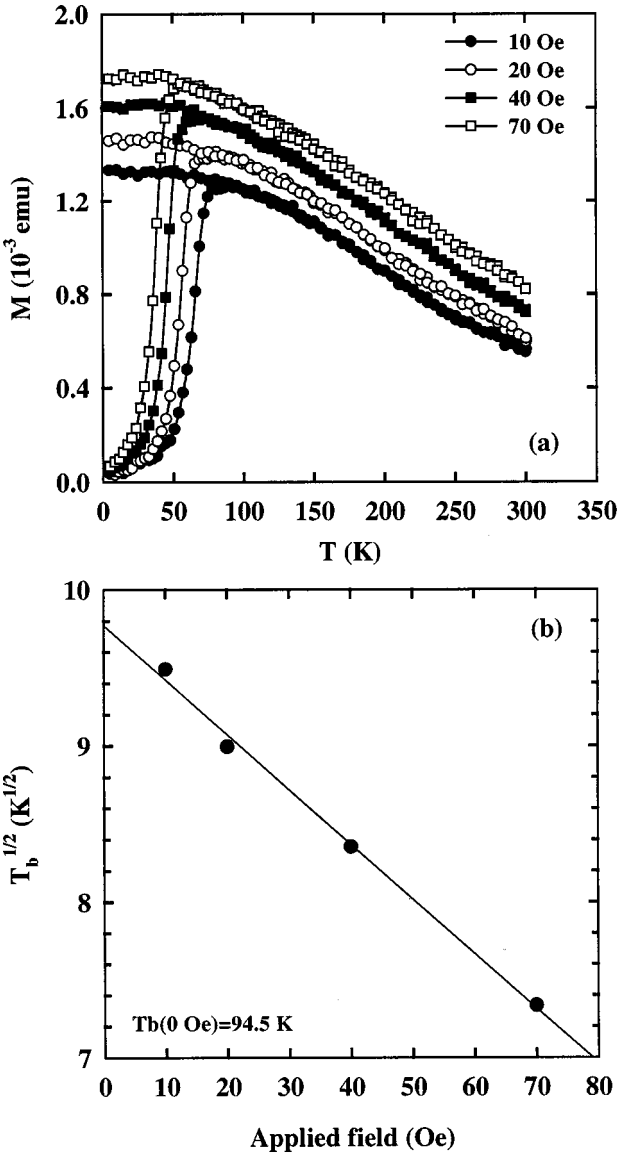

FIG. 5. (a) The temperature dependence of the magnetization for the irradiated (8×10^{14} Si^+/cm^2) sample, measured under conditions of (ZFC) and (FC) in several magnetic fields. (b) The variation of square root of the blocking temperatures ($T_b^{1/2}$) deduced from Fig. 5(a) as a function of the applied magnetic field. The line is a linear fit to the data.

The ZFC and FC data for the sample after a dose of 8×10^{14} Si^+/cm^2 is shown in Fig. 5(a) and the field dependence of the blocking temperature T_b is given in Fig. 5(b). A linear decrease of $T_b^{1/2}$ with H is found at this dose and also at other ion doses. It can be understood using the Chudnovsky[29] expression for the energy barrier in the presence of an applied field

$$E_B = KV\left[1-\left(\frac{\mu H}{2KV}\right)\right]^2. \tag{5}$$

Under the assumption that the energy barriers are determined only by the anisotropy energy KV, where K is the *total* anisotropy constant and V is the volume of the magnetic particles, the volume can be determined using the relation $KV \approx 25k_BT_b(H=0)$[30] for which the moment relaxation time

becomes comparable to the measurement period. Here $T_b(H=0)$ is the value of the blocking temperature extrapolated to zero field. Using $K=4.5\times10^5$ J/m^3 for the anisotropy constant of fcc Co, the mean diameter of the magnetic particles (considered spherical) were estimated from the calculated volume and are listed in Table I. The results of similar analyses after other ion doses are also given in Table I. From these data, it is evident that the particle-size distribution broadens and shifts to larger values as a function of ion dose.

Finally, for doses larger than 8×10^{15} Si$^+$/cm^2, the blocking temperatures become larger than room temperature and only a very small irreversibility is observed between FC and ZFC curves. It can be concluded that very large particles are formed under high-dose irradiation and/or large ferromagnetic regions are formed due to particle interactions. This conclusion is in agreement with the results obtained from the vibrating sample magnetometer measurements which show an important ferromagnetic contribution after irradiation greater than 10^{16} Si$^+$/cm^2.

D. Transport properties

1. Magnetoresistance measurements

At each stage of the irradiation process, magnetoresistance measurements were taken for two orientations of the magnetic field, perpendicular and parallel to the film surface. Measurements for different in-plane directions of the applied field indicated that the magnetoresistance was always isotropic in the plane. Figure 6 shows the magnetoresistance for the in-plane and perpendicular orientations for the sample (a) as deposited and (b) after irradiation with the largest dose of 5×10^{16} Si$^+$/cm^2. Ion bombardment has a dramatic effect on the magnitude of the magnetoresistance. In light of the magnetization data discussed earlier, this effect is consistent with the growth of the magnetic particles. In addition, the magnetoresistance of the high-dose sample saturates at a significantly lower field than the as-deposited one although there remains a significant difference between measurements in the two field orientations. It can be concluded that the initial shape anisotropy of the magnetic particles decreases strongly with ion bombardment but is not entirely eliminated even at the maximum ion dose.

The variations of the transport parameters $\rho(0)$, $\Delta\rho$, and $\Delta\rho/\rho(0)$ with ion dose are detailed in Figs. 7(a)–7(c); from them it is evident that a significant structural and magnetic evolution takes place on a scale comparable with the electron mean-free path ($\sim$50 Å). As shown in Fig. 7(a), the zero-field resistivity $\rho(0)$ increases initially by 25% for doses up to 8×10^{14} Si$^+$/cm^2, after which it passes through a maximum and decreases upon further irradiation to a value comparable to that of the as-deposited material. Since it has been demonstrated that the resistivity of the pure materials remains unaltered for similar ion treatment,[17] these variations must be related to the changes in the morphology resulting from ion irradiation. It should also be noted that the zero-field resistivities of granular $Ag_{1-x}Co_x$ (Ref. 10) are smaller than those of the metastable alloys with the same overall composition. With these points in mind, the initial increase

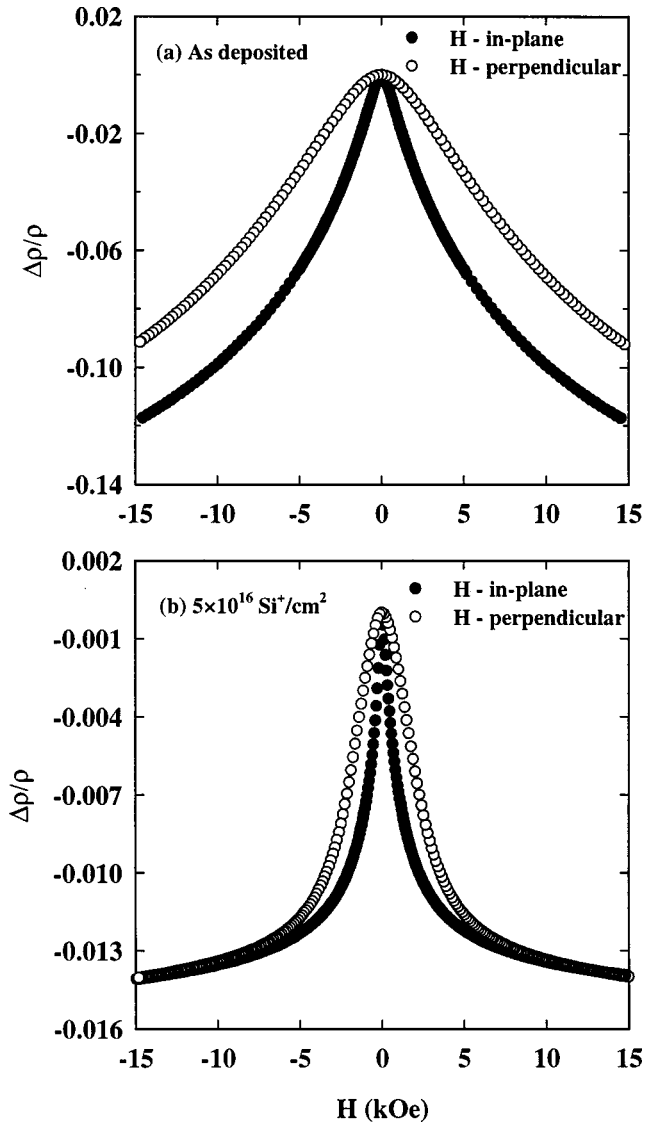

FIG. 6. Magnetoresistance $\Delta\rho/\rho$ at 300 K of the [50 Å(Co5 Å/Ag25 Å)$_{70}$] multilayer as a function of the magnetic field applied in the sample plane (filled circles) and perpendicular to the plane (open circles). (a) as-deposited and (b) after irradiation with 5×10^{16} Si$^+$/cm^2.

of the resistivity can be ascribed to a small amount of mixing near the Co/Ag interfaces. The decrease at larger doses then results from the formation and growth of magnetic Co particles. This picture is also supported by the decrease of the low-field slope in the $M-H$ curves in Fig. 3(a) followed by the onset of the hysteretic behavior as discussed previously.

The strong decrease of the $\Delta\rho$ upon irradiation, shown in Fig. 7(b), is also indicative of a change in the magnetic disorder on a scale of the order of the mean-free path. No significant changes are seen for doses lower than 1×10^{14} Si$^+$/cm^2, whereupon a slow decrease is observed up to a dose of 8×10^{14} Si$^+$/cm^2, followed by a more pronounced decrease at even higher doses. The combination of the variations in ρ and $\Delta\rho$ gives rise to the dependence of the GMR ($\Delta\rho/\rho$) shown in Fig. 7(c). The strong reduction of $\Delta\rho$ with dose can be explained on the basis of the phenomenological model proposed by Berkowitz *et al.*[6] and is also in agreement with the quantum theory proposed by Zhang and

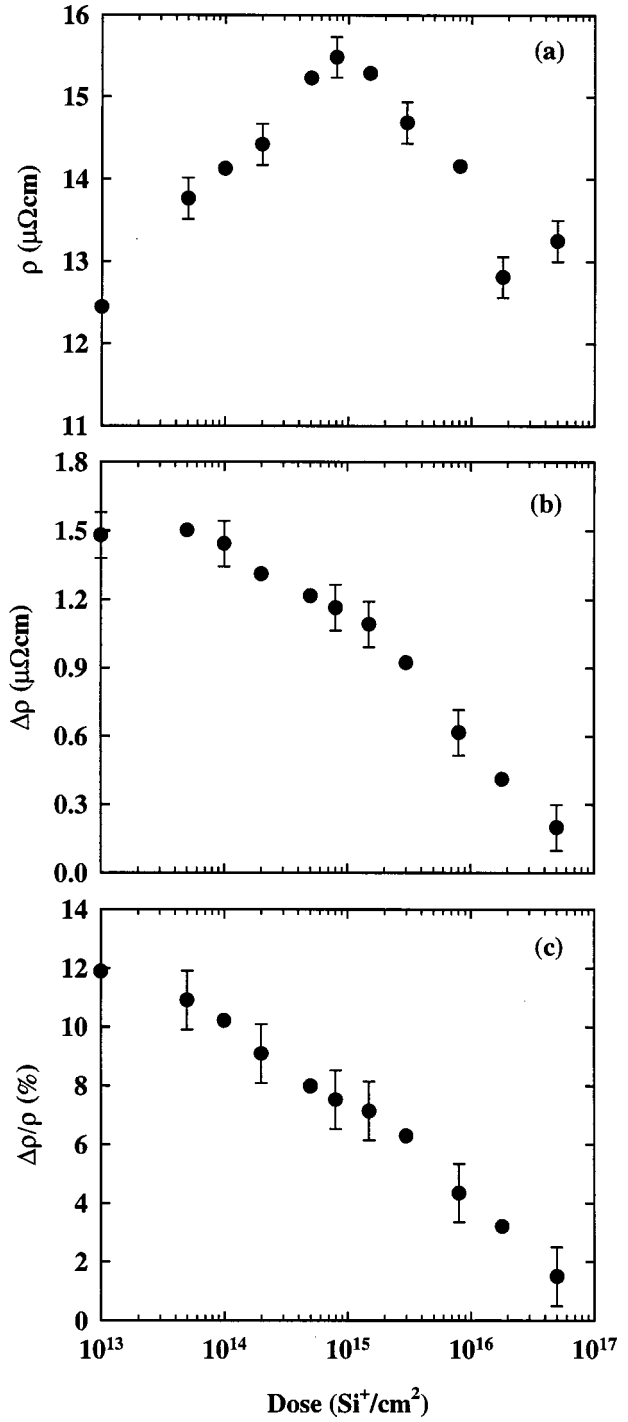

FIG. 7. The dependence of (a) the resistivity ρ, (b) its field change $\Delta\rho$, and (c) the magnetoresistance $\Delta\rho/\rho$ of the sample at 300 K as a function of the ion dose.

Levy.[7] Assuming that the spin-dependent ratio for scattering at grain surfaces is much larger than that within the magnetic grains, these models predict a decrease of $\Delta\rho/\rho$ with increasing particle size.

2. Analysis of the magnetoresistance

As Chien and co-workers[1,27] have emphasized, the key requirement for a significant GMR in granular magnetic alloys is the existence of nonaligned ferromagnetic single-domain particles separated by distances comparable with the electron mean-free path. The magnitude of the GMR has been found to be very sensitive to the size and concentration of ferromagnetic particles and to the presence of magnetic interactions between them. Parallel alignment of the particle moments (arising either from an external field or from positive interactions between particles) on a scale larger than the electron mean-free path will strongly reduce the GMR. Thus, information about the particle size distribution can be obtained from the magnetoresistance.

By symmetry[31,32] the magnetoresistance can be expressed as an even function of the reduced magnetization $m=M(H)/M_s$, where $M(H)$ is the global magnetization and M_s is the saturation value[33]

$$\frac{\Delta\rho}{\rho}=\frac{\rho(H)-\rho_0}{\rho_0}=-\alpha F\left(\frac{M(H)}{M_s}\right), \tag{6}$$

where $F(m)$ is an even function of m and the prefactor α sets the overall magnitude of the GMR. The simplest form for this function is a parabola ($F(m)=m^2$) valid for noninteracting moments; deviations from this simple dependence can arise due to the existence of weak magnetic interactions between particles.[32,34] In addition, a broad particle-size distribution can also lead to departures from the parabolic variation since small particles make a relatively larger contribution to the magnetoresistance than to the magnetization.[7]

Certain authors[5] have described the GMR in superparamagnetic systems using a bimodal distribution for the magnetic particles, reasoning that the moments of large particles will be more easily aligned than smaller ones at a given temperature. The large particles are then responsible for the low field variation of the magnetoresistance and small ones for the slow approach to saturation at high fields. In our case, the magnetization data have been analyzed on the basis of a log–normal distribution for the particles sizes [Eq. (4)], so the same approach has been employed to fit the magnetoresistance data. Specifically, Eq. (6) becomes

$$\frac{\Delta\rho}{\rho}=-\alpha\left(\int_{-\infty}^{\infty}L\left(\frac{\mu(D)H}{k_BT}\right)f(D)d(\ln D)\right)^2, \tag{7}$$

where $\rho(0)$ is the zero-field resistivity, $\Delta\rho$ the resistivity change in an applied field H, and α the amplitude of the GMR. As in Eq. (3), $L(x)$ is the Langevin function and $\mu=M_sV$ the magnetic moment of a particle with volume V.

The magnetoresistance curve following each irradiation was fitted to Eq. (7); the results of the fits for several doses are presented in Fig. 8. The as-deposited sample is characterized by a particle size distribution with $D_m=23$ Å and $\sigma=0.98$. The distribution broadens with dose and the mean-value D_m shifts up to 55 Å ($\sigma=0.72$) at the maximum dose of 5×10^{16} Si^+/cm^2. The values for the mean-particle diameter obtained from the fits are also listed in Table I. In Fig. 9 is plotted $\Delta\rho$ as a function of the inverse of the mean-particle size determined from the fits. For doses larger than 1.5×10^{15} Si^+/cm^2, $\Delta\rho\propto1/D_m$ as expected from the theoretical models[6,7] on the basis of independent superparamagnetic particles. However, for low doses $\Delta\rho$ deviates towards larger values. This deviation might arise from an overestimation of

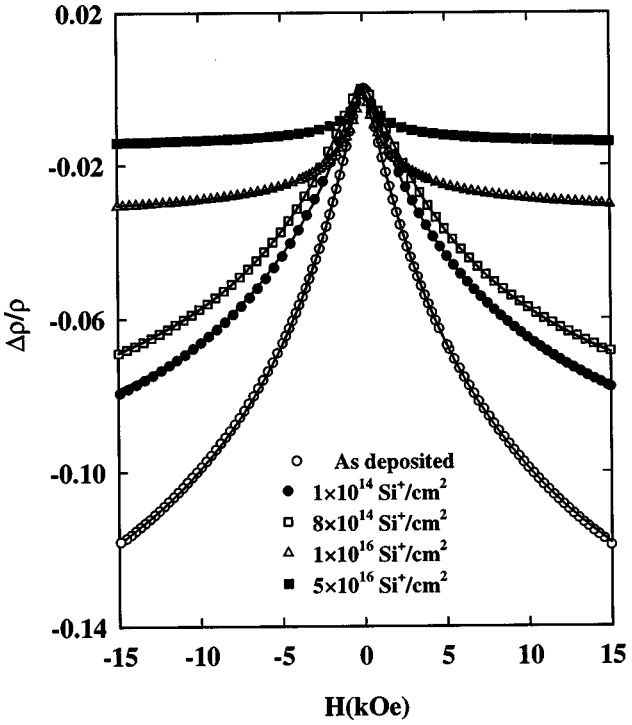

FIG. 8. Magnetoresistance for the sample at various ion doses. The solid lines are fits to the data, based on Eq. (7).

the size of anisotropic particles or from a possible magnetic coupling between Co particles across the Ag spacer, as Hylton *et al.*[2] have reported for their NiFe/Ag multilayers.

IV. DISCUSSION

Several mechanisms are generally invoked to describe ion-beam mixing/demixing in multilayers: collisional (ballistic) transport and irradiation-enhanced thermal diffusion.[35,36] Although the interplay between these mechanisms in different systems is not the subject of our article, it must be noted that the two mechanisms operate in opposite directions in the case of elements with large positive enthalpy of mixing.[37] Specifically, ballistic effects, which are always present, act as a mixing mechanism in the initial stages of the collision. For enhanced thermal diffusion, the energy lost by the primary ion generates atomic relocations in a cascade of nuclear collisions. The energy of the recoil atom is thermalized by secondary collisions down to kinetic energies of a few electron volts, comparable with chemical potentials in solids. At these energies the random walk atomic relocations can be chemically biased.[11] As noted from x-ray diffraction studies in Fe/Ag multilayers and bilayers,[12] chemically guided diffusion in systems with large positive heats of mixing provides a demixing mechanism during the thermal spike stage of the collision cascade.

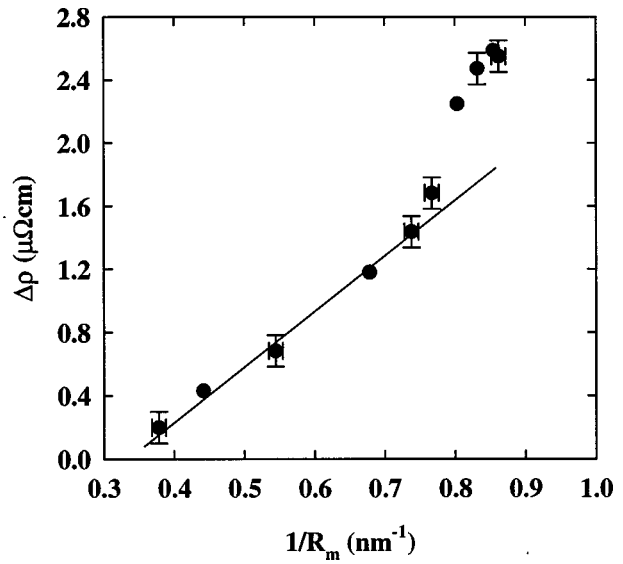

FIG. 9. The maximum change of the resistivity ($\Delta\rho=\alpha$) of the sample, obtained from the fits to the room temperature magnetoresistance, as a function of the inverse mean particle diameter. The solid line is a linear fit to the data for doses larger than 1.5×10^{15} Si^+/cm^2.

For thin Co-layer thicknesses, specifically 5 Å for our sample, the structural, magnetic, and transport data are consistent with a limited demixing near the Co/Ag interfaces at low ion doses followed by a progressive Co segregation at higher doses. As indicated in Table I, the mean-particle size almost doubles as a result of the ion irradiation. We can interpret these results as follows: At low doses, when there is no spatial superposition of the cascades, only short-range relocation within the collision cascade is possible so that the initial ballistic mixing is partially recovered by chemically driven relocation within the cascades. The role of chemical driving forces is enhanced for high doses when atomic relocations over extended regions due to the spatial superposition of cascades promote long range atomic migration and phase segregation.

It is also useful to compare the different results listed in Table I. For all doses, the distributions are quite broad ($\sigma=0.7-0.8$) indicating the presence of a wide range of particle sizes. Nevertheless, the values for the average particle size obtained through the analysis of the magnetization and transport data are surprisingly similar, given the fact that these properties are sensitive to different parts of the size distribution. In a broad size distribution, the major contribution to the low-field magnetization comes from large particles which make a relatively small contribution to the magnetoresistance. Large magnetic fields will align the moments of the smallest particles along with those of the large particles leading to relatively much smaller changes in the magnetization than in the magnetoresistance. As shown by Badia *et al.*,[38] the broad size distribution breaks down the simple parabolic relation between $\Delta\rho/\rho$ and $M(H)/M_s$ resulting in a field dependent prefactor $\alpha(H)$ in Eq. (7). At the same time, the particle radii obtained from the blocking temperature analysis are somewhat larger than those obtained from the other results. Since the blocking temperature depends on the energy barrier distribution whereas the superparamagnetism is coupled to the particle volume, these differences in particle sizes are to be expected for a broad size distribution.[39]

Qualitatively, the ion-induced evolution of the morphology reported here parallels the effect of thermal annealing of Co–Ag co-deposited alloys. Xiao *et al.*[40] demonstrate that thermal annealing of a $Co_{20}Ag_{80}$ alloy deposited at 77 K

induces growth of Co particles and a monotonic decrease in the magnetoresistivity change with the inverse magnetic-particle size, exactly as presented in Fig. 9. Since the interfacial area per unit volume is inversely proportional to the particle diameter for granular systems, this relationship underscores the importance of interfacial scattering for the magnetoresistance. In this context, both ion-beam and thermal treatments are controlled by the thermodynamics of these mixtures as outlined in the Introduction. At the relatively high ion doses employed in the present experiments, the principal effect of high-energy ion bombardment on the evolution of the morphology of Co/Ag multilayers is thermal, albeit on a very local scale. This conclusion contrasts that found for low-dose ion irradiation of Co/Cu multilayers of similar thicknesses[16] where ion bombardment initially mixes the layers and thermal annealing reversibly demixes them.

ACKNOWLEDGMENTS

The authors would like to thank Dominic Ryan of McGill University for access to his low temperature magnetometer and to him and Li Cheng for assistance with the measurements. They also acknowledge Mokhtar Rouabhi for helpful discussions as well as S. Germain and F. Schiettekatte for their assistance with the ion-beam experiments, G. Rinfret and R. Rinfret for the maintenace of the sputtering and magnetoresistance equipment, and P. Bérichon and R. Gosselin for help with the operation of the tandem accelerator. This research has been supported by the NSERC of Canada and le Fonds FCAR du Quebec.

[1] C. L. Chien, J. Q. Xiao, and J. S. Jiang, J. Appl. Phys. **73**, 5309 (1993).
[2] T. L. Hylton, K. R. Coffey, M. A. Parker, and J. K. Howard, Science **261**, 1021 (1993).
[3] O. Redon, J. Pierre, B. Rodmacq, B. Mevel, and B. Dieny, J. Magn. Magn. Mater. **149**, 398 (1995); B. Dieny, S. R. Teixeira, B. Rodmacq, C. Cowache, S. Auffret, O. Redon, and J. Pierre, J. Magn. Magn. Mater. **130**, 197 (1994).
[4] W. H. Flores, S. R. Teixeira, J. Geshev, J. B. M. da Cunha, P. J. Schilling, A. Traverse, and M. C. Martins Alves, J. Magn. Magn. Mater. **188**, 17 (1998).
[5] T. Luciñski and F. Stobiecki, Phys. Status Solidi A **163**, 195 (1997).
[6] A. Berkowitz, J. R. Mitchell, M. J. Carey, A. P. Young, S. Zhang, F. E. Spada, F. T. Parker, A. Hutten, and G. Thomas, Phys. Rev. Lett. **68**, 3745 (1992).
[7] S. Zhang, Appl. Phys. Lett. **61**, 1855 (1992); S. Zhang and P. Levy, J. Appl. Phys. **73**, 5315 (1993).
[8] T. A. Rabedeau, M. F. Toney, R. F. Marks, S. S. P. Parkin, R. F. C. Farrow, and G. R. Harp, Phys. Rev. B **48**, 16 810 (1993).
[9] L. Z. Mezey and H. Giber, Jpn. J. Appl. Phys., Part 1 **21**, 1569 (1982).
[10] J. Q. Xiao, J. S. Jiang, and C. L. Chien, IEEE Trans. Magn. **29**, 2688 (1993).
[11] B. M. Paine and R. S. Averbach, Nucl. Instrum. Methods Phys. Res. B **7/8**, 666 (1985).
[12] A. C. Sosa, P. Schaaf, W. Bolse, K. P. Lieb, M. Gimbel, U. Geyer, and C. Tosello, Phys. Rev. B **53**, 14 795 (1996).
[13] J. Pacaud, G. Gladyszewski, C. Jaouen, A. Naudon, Ph. Gondeau, and J. Grilhé, J. Appl. Phys. **73**, 2786 (1993).
[14] H. U. Krebs, Y. Luo, M. Störmer, A. Crespo, P. Schaaf, and W. Bolse, Appl. Phys. A: Mater. Sci. Process. **61**, 159 (1995).
[15] V. Kornievski, K. V. Rao, D. M. Kelly, I. K. Shuller, K. K. Larsen, and J. Bøttiger, J. Magn. Magn. Mater. **140–144**, 549 (1995); D. M. Kelly, I. K. Schuller, V. Kornievski, K. V. Rao, K. K. Larsen, J. Bøttiger, E. M. Gyorgy, and R. B. van Dover, Phys. Rev. B **50**, 3481 (1994).
[16] M. Cai, T. Veres, S. Roorda, R. W. Cochrane, R. Abdouche, and M. Sutton, Mater. Res. Soc. Symp. Proc. **504**, 197 (1998).
[17] T. Veres, M. Cai, S. Germain, M. Rouabhi, F. Schiettekatte, S. Roorda, and R. W. Cochrane, J. Appl. Phys. **87**, 8503 (2000).
[18] Y. Huai, Ph.D. thesis, Université de Montréal, 1993.
[19] R. W. Cochrane, B. J. Kastner, and W. B. Muir, J. Phys. E **15**, 425 (1982).
[20] A. Berkowitz, J. R. Mitchell, M. J. Carey, A. P. Young, D. Rao, A. Starr, S. Zhang, F. E. Spada, F. T. Parker, A. Hutten, and G. Thomas, J. Appl. Phys. **73**, 5320 (1993).
[21] B. E. Warren, *X-Ray Diffraction* (Addison-Wesley, Reading, MA, 1969), p. 253.
[22] M. B. Stearns and Y. Cheng, J. Appl. Phys. **75**, 6894 (1994).
[23] C. L. Chien, J. Appl. Phys. **69**, 5267 (1991).
[24] R. W. Chantrell, J. Popplewell, and S. W. Charles, IEEE Trans. Magn. **14**, 975 (1978).
[25] F. E. Luborsky, J. Appl. Phys. **32**, 171S (1961).
[26] J. R. Childress and C. L. Chien, J. Appl. Phys. **70**, 5885 (1991).
[27] J. R. Childress and C. L. Chien, Appl. Phys. Lett. **56**, 95 (1991).
[28] S. H. Liou, S. Malhorta, Z. S. Shan, D. J. Sellmyer, S. Nafis, J. A. Woollam, C. P. Reed, R. J. De Angelis, and G. M. Chow, J. Appl. Phys. **70**, 5882 (1991).
[29] E. Chudnovsky, J. Appl. Phys. **73**, 6697 (1993).
[30] B. D. Cullity, *Introduction to Magnetic Materials* (Addison-Wesley, Reading, MA, 1972), p. 410.
[31] J. I. Gitteleman, Y. Goldstein, and S. Bosowski, Phys. Rev. B **5**, 360 (1972).
[32] M. R. Parker, J. A. Barnard, D. Seale, and A. Wakins, J. Appl. Phys. **73**, 5512 (1993).
[33] J. Q. Xiao, J. S. Jiang, and C. L. Chien, Phys. Rev. Lett. **68**, 3749 (1992).
[34] P. Allia, M. Knobel, P. Tiberto, and F. Vinai, Phys. Rev. B **52**, 15 398 (1995).
[35] W. L. Johnson, Y. T. Cheng, M. Van Rossum, and M.-A. Nicolet, Nucl. Instrum. Methods Phys. Res. B **7/8**, 657 (1985).
[36] P. Sigmund and A. Gras-Marti, Nucl. Instrum. Methods Phys. Res. **182–183**, 25 (1981).
[37] D. Marton, J. Fine, and G. P. Chambers, Phys. Rev. Lett. **61**, 2697 (1988).
[38] F. Badia, X. Batlle, A. Labarta, M. L. Watson, A. B. Johnston, and J. N. Chapman, J. Appl. Phys. **82**, 677 (1997).
[39] E. Vincent, Y. Yuan, J. Hammann, H. Hurdequint, and F. Guevara, J. Magn. Magn. Mater. **161**, 209 (1996).
[40] J. Q. Xiao, J. S. Jiang, and C. L. Chien, Mater. Res. Soc. Symp. Proc. **286**, 197 (1993).